Tellus (1987), *39A*, 460–473

Exploratory studies of cloud radiative forcing with a general circulation model

By ROBERT D. CESS, *Laboratory for Planetary Atmospheres Research, State University of New York, Stony Brook, New York 11794, USA*, and GERALD L. POTTER, *Lawrence Livermore National Laboratory, University of California, Livermore, CA 94550, USA*

(Manuscript received 22 October; in final form 15 December 1986)

ABSTRACT

Cloud radiative forcing constitutes the radiative impact of clouds upon the earth's present climate, while cloud radiative feedback is the change in this forcing associated with climatic change. The present study addresses two issues concerning cloud radiative forcing. The first is that an intercomparison of cloud radiative forcing, as predicted by six different general circulation models, shows a considerable lack of agreement, underscoring the need for an improved understanding of cloud/radiation interactions within such models. The second issue pertains to an examination of strategies by which model-predicted cloud/radiation interactions should be compared with satellite-derived data sets.

1. Introduction

Observed and projected increases in atmospheric carbon dioxide, as a consequence of fossil fuel burning, have stimulated considerable interest in modeling future climatic change associated with this perturbation upon atmospheric composition. The most detailed numerical climate models for this purpose are three-dimensional general circulation models (GCMs). But as illustrated by Schlesinger (1984) and Schlesinger and Mitchell (1985), an intercomparison of several general circulation model predictions shows quite differing climatic responses to increasing atmospheric CO_2.

Any attempt towards understanding the reasons for these differences will require a systematic examination of individual parameterizations and processes within the models. Certainly one such process that necessitates examination is the radiative impact of clouds upon climate. Recently there have been strategies suggested by which cloud/climate interactions within models can be tested (Ramanathan, 1983; 1985; Hartman et al., 1986; Ramanathan, 1987). These strategies specifically pertain to the use of satellite data to validate model-predicted cloud radiative forcing.

In the following, cloud radiative forcing refers to the impact of clouds upon the earth's radiation budget as determined at the top of the atmosphere (e.g., Charlock and Ramanathan, 1985). Choosing illustrative hypothetical numbers, if the enhanced reflection of solar radiation due to clouds leads to a reduction of 50 Wm^{-2} in solar absorption by the earth-atmosphere system, while the greenhouse effect of clouds produces a 25 Wm^{-2} infrared warming of that system, then the net cloud forcing is -25 Wm^{-2}; i.e., a 25 Wm^{-2} cooling of the earth-atmosphere system.

The important point here is that we need to understand cloud radiative forcing in order to understand cloud radiative feedback. Again a simple example serves to illustrate this point. Basically, climatic change associated with a doubling of atmospheric CO_2 is a response to a 4 Wm^{-2} CO_2-induced warming of the surface-troposphere system. But if this climatic change in turn alters cloud radiative forcing, through changes in cloud amount, optical properties and vertical structure, from $-25\ Wm^{-2}$ to $-21\ Wm^{-2}$, again using hypthetical numbers, the initial surface-troposphere heating of $4\ Wm^{-2}$ would then be amplified to $8\ Wm^{-2}$. The ensuing climatic change, for this hypothetical situation, would thus be roughly doubled due to cloud radiative feedback.

As summarized by Wetherald and Manabe (1986), GCM simulations do in fact indicate climate-induced changes in cloud amount and vertical structure, and that positive cloud feedback operates within certain of the simulations. These simulations do not, however, incorporate climate-induced changes in cloud optical properties, an effect that Petukhov et al. (1975), Paltridge (1980), and Somerville and Remer (1984) suggest could produce negative feedback. On the other hand, Charlock (1982) has suggested that even the sign of this feedback might be uncertain. But, as previously emphasized, the prerequisite to understanding cloud radiative feedback is to first understand cloud radiative forcing.

A further important point is that one must not confuse cloud radiative feedback with cloud radiative forcing. For example, several empirical studies have appeared (e.g., Cess, 1976; Ohring and Clapp, 1980; Hartmann and Short, 1980; Cess et al., 1982) which do not explicitly indicate whether they are attempting to analyze forcing or feedback. The work by Cess (1976) serves as an example of this confusion, since he simultaneously treated solar cloud forcing and infrared cloud feedback. Distinctions between infrared forcing and infrared feedback have been emphasized by Cess and Ramanathan (1978).

The purpose of the present paper is to point out several aspects of cloud radiative forcing. First, a radiative-convective model will be employed to illustrate certain features of cloud/climate interactions. Following this, an intercomparison of cloud radiative forcing as predicted by several GCMs will demonstrate the need for improving our understanding as to how clouds impact a GCM's climate. To further emphasize this point, the Oregon State University/Lawrence Livermore National Laboratory GCM (OSU/LLNL GCM) will be employed for the purpose of illustrating sensitivity of the model's cloud radiative forcing to certain of the model's physical processes. Next, pitfalls associated with GCM and satellite data intercomparisons will be emphasized. This is accomplished by utilizing the OSU/LLNL GCM in conjunction with the GOES (Geostationary Operational Environmental Satellite) radiation budget data of Minnis and Harrison (1984b) which distinguishes between clear and overcast regions.

2. Cloud/climate interactions

Before proceeding, it is useful to employ the radiative-convective model (RCM) analog of the OSU/LLNL GCM for the purpose of clarifying certain aspects of cloud/climate interactions. This RCM is described by Cess et al. (1985), and it comprises modifications made by S. J. Ghan (Cess et al., 1985) to an earlier version developed by M. E. Schlesinger (Hall et al., 1982).

The first point concerns the separate solar and infrared contributions to the impact of clouds upon climate. The solar contribution is predominantly one of surface cooling, whereas the infrared contribution manifests itself largely as a tropospheric heating. This different partitioning between surface and troposphere has the potential for significantly altering the atmospheric structure. In particular, Ramanathan (1987) has emphasized that cloud-induced surface solar cooling and atmospheric infrared warming will tend to stabilize the atmospheric column, which will in turn influence the way that clouds impact the surface climate.

To illustrate this, we have performed a simulation with the RCM to show the impact of one specific cloud upon the RCM's surface energy budget. The approach here is analogous to Ramanathan's (1981) elucidation of the physical processes that govern climatic warming due to increasing atmospheric CO_2. The single cloud is located within the 200–400 mb layer, it has an infrared emissivity of 0.5, and the wavelength dependent asymmetry factor and single scattering albedo are as given by Cess et al. (1985, their cloud type CL_1). Two simulations were performed, one for clear skies and the other with the 200–400 mb cloud present. For purposes of illustration, the visible optical depth of the cloud, τ, was chosen so that the model's surface temperature was the same with or without the presence of the cloud, i.e., the solar and infrared cloud/

climate impacts compensate one another. This produced $\tau = 1.885$.

The changes in the components of the model's surface energy budget are summarized within Table 1, where a positive quantity represents energy added to the surface. After incorporating the cloud into the model, the RCM was run through a single time step so as to isolate the direct radiative impact of the cloud with all other climate parameters remaining at their original (i.e., clear-sky) values. As would be expected, the dominant effect here is that of cloud-induced solar cooling of the surface. But when the model is subsequently run to equilibrium, and recall that the cloud produces no change in the model's equilibrium surface temperature, the corresponding increase in atmospheric static stability results in an increase in atmospheric infrared emission from the atmosphere to the surface, together with reducing the latent and sensible heat losses from the surface. Thus it is these response processes which largely compensate for the direct 56.7 Wm^{-2} reduction in surface solar absorption.

The point is that one must be careful to distinguish between direct as opposed to equilibrium changes when interpreting the impact of clouds upon climate. Moreover, the results of Table 1 clearly illustrate the importance of surface processes upon cloud/climate interactions.

A further important point concerns conceptual interpretations as to how a given model's climate responds to a change in the radiative impact of the model's clouds. To illustrate this, we have performed two climate-change simulations with the RCM, taking as the control climate that for which the 200–400 mb cloud is present. One simulation is for a doubling of atmospheric CO_2, which produces a 3.9 Wm^{-2} direct heating of the surface-troposphere system, while the second simulation is to change the radiative impact of the cloud by lettering $\Delta\tau = -0.171$, which also produces 3.9 Wm^{-2} direct heating of the surface-troposphere system. The partitioning of this heating between surface and troposphere is, however, significantly different for the two simulations, as seen from the results summarized in Table 2.

The corresponding changes in equilibrium surface quantities are summarized in Table 3. Note that, despite the differences in the individual energy flux changes, the two simulations produce nearly identical changes in the total energy added to the surface, and hence also the change in surface temperature. The point, as has been emphasized by others (e.g., Ramanathan et al., 1979; Dickinson, 1982; Potter and Cess, 1984), is that a model's climate responds to the direct surface-troposphere perturbation, irrespective as to how this perturbation is partitioned between surface and troposphere. Certain caveats to this conclusion are given by Cess et al. (1985), but they are not germane to the present investigation.

Table 1. *Changes in the components of the RCM's surface energy budget as induced by the presence of the 200–400 mb cloud*

	Surface flux change (Wm^{-2})	
Component	direct	equilibrium
absorbed solar	−56.7	−59.1
absorbed infrared	20.2	36.8
latent plus sensible	0	22.3
total	−36.5	0

Table 2. *Direct radiative heating (Wm^{-2}) of the RCM's surface, troposphere and surface-troposphere due to a doubling of CO_2 and a reduction in cloud visible optical depth*

System	$2 \times CO_2$	$\Delta\tau = -0.171$
Surface	1.77	3.42
troposphere	2.13	0.48
surface-troposphere	3.90	3.90

Table 3. *Changes in the RCM's equilibrium surface quantities for a doubling of CO_2 and a reduction in cloud visible optical depth*

Change in:	$2 \times CO_2$	$\Delta\tau = -0.171$
absorbed solar (Wm^{-2})	−1.12	2.30
absorbed infrared (Wm^{-2})	16.82	14.81
latent plus sensible (Wm^{-2})	−4.29	−5.38
total of above (Wm^{-2})	11.41	11.71
surface temperature (°C)	1.89	1.94

In the above example, the $\Delta\tau = -0.171$ simulation serves as a sort of analog to cloud feedback which, as discussed in the Introduction, comprises a climate-induced change in cloud radiative forcing, but with the distinction here that cloud radiative forcing refers to the surface-troposphere system, in contrast to the radiation budget at the top of the atmosphere as defined in the Introduction. But there should be little difference in cloud forcing as determined at the tropopause or at the top of the atmosphere.

To illustrate this, lettering CF denote cloud radiative forcing, the separate infrared and solar components, CF(infrared) and CF(solar), may be expressed as (e.g., Charlock and Ramanathan, 1985; Hartmann et al., 1986; Ramanathan, 1987)

$$\text{CF(infrared)} = F(\text{clear}) - F(\text{total}) \quad (1)$$

$$\text{CF(solar)} = S(\text{total}) - S(\text{clear}) \quad (2)$$

where F and S denote, respectively, the upward emitted infrared flux and the net incident solar flux at the top of the atmosphere, while clear and total respectively refer to clear and to clear plus overcast conditions. But CF as determined from eqs. (1) and (2) should be equally applicable to the surface-troposphere system, since the overlying stratospheric contribution is quite insensitive as to whether the troposphere is clear or cloudy, and thus this contribution cancels within eqs. (1) and (2). So, for all practical purposes, satellite-inferred cloud radiative forcing may be interpreted as referring to the surface-troposphere system.

Ideally, agreement between model-predicted and satellite-observed cloud radiative forcing should serve to validate the way in which clouds impact a model's climate. But as illustrated in later sections, there is always the potential for compensating errors, so that such agreement should be regarded as a necessary but not sufficient condition for model validation.

3. General circulation model description

For present purposes the two-level OSU/LLNL GCM will be employed strictly as an educational vehicle for the purpose of elucidating certain aspects of cloud radiative forcing as computed by a GCM. Given the uncertainties of GCM generated cloud interactions in general, and the limitations to such an endeavor with a two-level model in particular, there is no intent to employ the GCM in a predictive mode relative to cloud radiative forcing.

The OSU/LLNL GCM is a modified version of the Oregon State University GCM (OSU GCM), with a description of the latter being given by Ghan et al. (1982). This modification evolved in two stages. The first-stage modification consisted of replacing the solar radiation routine within the OSU GCM by a delta-Eddington model (Cess et al., 1985). As in the original model, the solar spectrum was divided, at 0.9 μm, into two wavelength intervals.

The second-stage modification incorporated the following changes:

- The $\lambda < 0.9$ μm wavelength interval was further subdivided, at 0.5 μm, into two intervals.
- Although solar absorption by ozone is included in the original OSU GCM, it was ignored in the first-stage modification of the model (Cess et al., 1985). This has presently been incorporated into the delta-Eddington routine by using the separate UV and visible ozone absorption parameterizations of Lacis and Hansen (1974) for the respective $\lambda < 0.5$ μm and $\lambda = 0.5$ to 0.9 μm wavelength intervals. Zonal and seasonal ozone amounts are from the OSU GCM (Ghan et al., 1982).
- The ocean albedo, which is a parameterization to Fresnel reflection in the OSU GCM (Ghan et al., 1982), has been replaced by the ocean albedo model of Briegleb et al. (1986). This produces a darker ocean at large solar zenith angles.

Although the OSU/LLNL GCM has only two interior tropospheric levels and thus no stratospheric simulation, the model does contain a non-interactive stratosphere. Hence the model differentiates between radiative fluxes at the tropopause (200 mb) and those at the top of the atmosphere.

The present OSU/LLNL GCM simulations consist of 90-day perpetual-month integrations with average insolation and prescribed sea-surface temperatures for the specified month. Sea-surface temperatures are from Alexander and Mobley (1976). Averaging is performed over the last 30 days of the 90-day run.

In the following, we employ the OSU/LLNL GCM in two different roles. First, it is utilized as one of six GCMs for the purpose of intercomparing GCM-predicted cloud radiative forcing. But more importantly, it is then employed as a vehicle for understanding certain aspects of cloud/radiation interactions, and for examining strategies by which GCM-predicted cloud/radiation interactions should be compared with satellite derived data sets.

4. Cloud radiative forcing

Table 4 summarizes global-mean cloud radiative forcing, together with its infrared and solar components, as predicted by five different GCMs in addition to our present simulations with the OSU/LLNL GCM. These comprise the GLAS (NASA Goddard Laboratory for Atmospheric Sciences) GCM, two versions of the NCAR CCM (National Center for Atmospheric Research Community Climate Model), the UCLA/Goddard (University of California Los Angles/NASA Goddard Space Flight Center) GCM, and the UKMO (United Kingdom Meteorological Office) GCM. The modified NCAR CCM (Charlock and Ramanathan, 1985) utilized internally generated cloud optical properties while, with one exception, the other GCMs employed prescribed cloud optical properties. The exception is the version of the NCAR CCM used by Ramanathan (1987), within which a liquid-water scaled cirrus cloud emissivity was adopted (Ramanathan, 1985).

The results summarized within Table 4 refer to simulations for a specified month (January or July), employing prescribed sea surface temperatures for that month. To facilitate January/July comparisons, insolation differences due to the earth's eccentric orbit have been removed by correcting CF(solar) to a mean sun-earth distance. Clearly there is a lack of agreement amongst the different models, with the greatest discrepancies occurring for the infrared component of cloud forcing. These comparisons certainly emphasize the need for improving our understanding as to how to model the impact of clouds upon climate within a GCM.

Note the increase in total cloud forcing for January vs July, as indicated by the GCMs for which both January and July simulations have been performed. While it is tempting to attribute this to a seasonal cloud radiative feedback, most of the change is contained in the solar component. A plausible explanation for this effect is that the Southern Hemisphere has a lower surface albedo (due to greater ocean extent) than does the

Table 4. *Intercomparison of cloud radiative forcing as predicted by several general circulation models; the seasonal solar forcing has been corrected to the mean sun-earth distance*

	Cloud radiative forcing (Wm^{-2})		
Reference	infrared	solar	total
Herman et al. (1980)			
GLAS GCM, Jan.	40	−54	−14
Charlock & Ramanathan (1985)			
Modified NCAR CCM, Jan.	23	−45	−22
Ramanathan (1987)			
NCAR CCM, Jan.	35	−57	−22
Randall & Harshvardhan (1986)			
UCLA/Goddard GCM, Jan.	55	−57	−2
UCLA/Goddard GCM, July	53	−52	+1
Mitchell (Personal communication, 1986)			
UKMO GCM, Jan.	40	−74	−34
UKMO GCM, July	42	−69	−27
Present study			
OSU/LLNL GCM, Jan.	42	−62	−20
OSU/LLNL GCM, July	39	−52	−13

Northern Hemisphere. Consequently clouds should exert a greater cooling effect upon the Southern Hemisphere as opposed to the Northern Hemisphere, a conclusion which is consistent with the UKMO GCM simulation by Slingo (1982, her Fig. 7). When insolation weighting is taken into account, this would result in January/July global-mean CF(solar) differences which are consistent in direction with the results of Table 4.

Before proceeding, it is necessary to address differences in the way cloud radiative forcing has been evaluated in the various GCM simulations. In the case of Herman et al. (1980), the separate infrared and solar components of cloud forcing were determined by performing three GCM simulations; a standard control run plus two simulations in which cloud infrared and solar opacities were respectively set equal to zero. These latter two simulations thus contain different meteorology than in the standard control run, resulting in a computational procedure which is at variance with our concept of cloud radiative forcing. We have made no attempt to estimate the consequences of this procedure.

In the simulations by Charlock and Ramanathan (1985) and Ramanathan (1987), the NCAR CCM computes fractional cloudiness at each gridpoint, and the clear-sky fluxes were separately binned during the GCM simulation. They then took these clear-sky fluxes to be representative of the entire region depicted by the given gridpoint. Thus their method of computing clear-sky fluxes refers to combined clear/overcast atmospheric conditions. For later purposes, we refer to this manner of evaluating cloud radiative forcing as Method II.

Although the UCLA/Goddard GCM does not compute fractional cloudiness, in their simulations Randall and Harshvardhan (1986) performed two radiative computations for overcast gridpoints; one with clouds present (which was employed as a predicted quantity within the model), and one with clouds removed which was then combined with the fluxes computed at clear gridpoints. Thus despite the different manners in which cloud cover is computed within the NCAR CCM and the UCLA/Goddard GCM, the procedure of Randall and Harshvardhan (1986) is consistent with Method II.

Like the UCLA/Goddard GCM, the OSU/LLNL GCM does not compute fractional cloudiness. But in contrast to Randall and Harshvardhan (1986), our clear-sky fluxes refer strictly to clear gridpoints, and this will be referred to as Method I. The UKMO GCM, like the NCAR CCM, computes fractional cloudiness at each gridpoint, and Mitchell (Mitchell, J. F. B., 1986, personal communication) employed the same procedure as did Charlock and Ramanathan (1985), such that his results are consistent with Method II.

Shortly we shall employ the OSU/LLNL GCM to illustrate differences between Method I and Method II evaluations of cloud radiative forcing. But before doing so it is useful to make two points concerning Method I vs Method II. The first point concerns conceptual difficulties in relating cloud radiative forcing as determined by a GCM to that as measured by satellite instruments, due to the considerable differences in spatial resolution between GCMs and satellite observations. For example, with respect to geographical areas containing broken cloudiness one can argue that both methods should produce comparable results, since here there is probably little difference between clear and overcast atmospheric conditions. But if the area of broken cloudiness is depicted by either the ULCA/Goddard or OSU/LLNL GCMs as completely overcast, due to these models not computing fractional cloudiness, then Method II might be preferable. Conversely, Method I would appear to be the most applicable for geographical areas which simultaneously contain extended clear and extended overcast regions.

Returning to the question of differences between Method I and Method II determinations, we have employed Randall and Harshvardhan's (1986) procedure to obtain Method II cloud forcing with the OSU/LLNL GCM. Global-mean results are summarized in Table 5, and here there is little difference between the two computational procedures.

There are, however, differences in zonal-mean cloud infrared forcing as is illustrated in Figs. 1 and 2, and note specifically the January/July reversal in this difference at high northern latitudes. Inspection of the model's cloud cover indicates that this is due to the model producing extended clear regions over Asia together with extended overcast regions over ocean areas. Since

Table 5. *Comparison of the OSU/LLNL GCM predicted cloud radiative forcing utilizing both Method I and Method II; the January and July solar forcings have been corrected to the mean sun-earth distance*

	Cloud radiative forcing (Wm^{-2})		
Simulation	infrared	solar	total
Jan., Method I	41.5	−61.8	−20.3
Method II	43.4	−62.8	−19.4
July, Method I	38.8	−52.4	−13.6
Method II	37.5	−52.8	−15.3

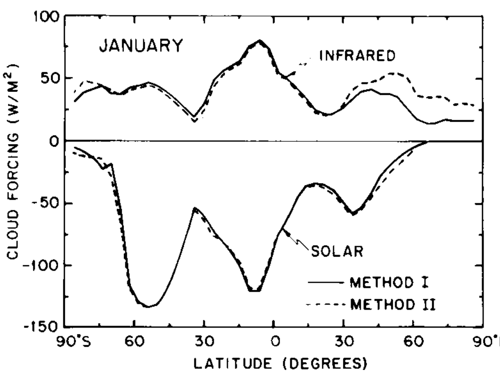

Fig. 1. A comparison of Methods I and II evaluations of cloud radiative forcing for January. These results were obtained using the OSU/LLNL GCM.

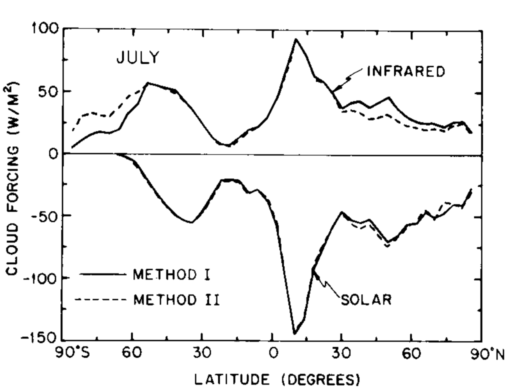

Fig. 2. A comparison of Methods I and II evaluations of cloud radiative forcing for July. These results were obtained using the OSU/LLNL GCM.

Method II computes clear-sky fluxes for both clear and overcast regions, then in January this clear-sky flux is enhanced by the ocean/overcast contribution, since the oceans are warmer than the extended clear regions over Asia. In July this effect is reversed.

Within the confines of the comparisons shown in Figs. 1 and 2, together with our prior suggestion that Method I is preferable for geographical areas that contain both extended clear and extended overcast regions, one might conclude, for purposes of comparison with satellite data, that Method I is the more correct of the two procedures. But we also suggested that Method II might be the more appropriate for regions of broken cloudiness, and the OSU/LLNL GCM is not appropriate for testing this suggestion since it does not compute fractional cloud cover. It would appear useful to additionally investigate Method I/II differences by employing a GCM which does compute fractional cloudiness.

Aside from differences in the manner by which cloud radiative forcing is calculated, a potential source of disagreement among individual GCM simulations is that some models contain a diurnal cycle while others do not. For example, four GCMs have routinely been used to study the CO_2-climate problem: the NCAR CCM, the OSU GCM, the GFDL (NOAA Geophysical Fluid Dynamics Laboratory) GCM, and the GISS (NASA Goddard Institute for Space Studies) GCM. Of these, the OSU and GISS GCMs contain a diurnal cycle, whereas the others employ a "fixed-sun" approximation in which a latitudinally-dependent mean solar zenith angle is employed which produces the correct diurnally-averaged insolation.

Only recently has the fixed-sun approximation been appraised. Employing the UCLA GCM (which contains an earlier radiation code than does the UCLA/Goddard GCM), Randall et al. (1985) performed July simulations with the fixed-sun approximation together with the standard diurnal-cycle version of the model. As they point out, the diurnal cycle has a strong effect upon the energy budgets at both the top of the atmosphere and at the surface, and upon the partitioning of July precipitation between continents and oceans. To cite a specific example, their planetary albedo increased from 0.28 to 0.31 when the diurnal cycle was suppressed. As Randall et al.

(1985) conclude, "the diurnal cycle cannot be neglected as a detail, even for climate simulations."

To further emphasize this conclusion, we have performed a fixed-sun simulation with the OSU/LLNL GCM. Cloud forcing results are summarized in Table 6 for July simulations, and note in particular the impact that the fixed-sun approximation has upon the solar component of cloud forcing. This raises an interesting point. If, for intercomparison purposes, we only had results for the NCAR CCM and the OSU/LLNL GCM, then from Table 4 we would conclude that the two models produce rather consistent infrared and solar components of cloud radiative forcing. But Table 6 suggests that this consistency would be fortuitous, since the OSU/LLNL GCM contains a diurnal cycle while the NCAR CCM does not.

Moreover, inclusion or exclusion of the diurnal cycle does not resolve the lack of agreement within Table 4. The UCLA/Goddard, UKMO and OSU/LLNL GCMs all contain a diurnal cycle, and with reference to Table 5 they employ reasonably consistent definitions of cloud radiative forcing. But the lack of agreement nevertheless persists.

To illustrate causes of the diurnal-cycle versus fixed-sun differences, zonal-mean flux errors at the top of the atmosphere, defined as fixed-sun flux minus diurnal-cycle flux, are illustrated in Fig. 3. The correlation between positive solar errors and negative infrared errors is consistent with differences in cloud cover. But as Randall et al. (1985) point out, there are further subleties associated with the absence of day/night cloud-cover variations in the fixed-sun simulation.

Table 6. *Comparison of the OSU/LLNL GCM predicted cloud radiative forcing employing a diurnal cycle and with the fixed-sun approximation; the July solar forcing has been corrected to the mean sun-earth distance*

	Cloud radiative forcing (Wm^{-2})		
Mode of operation	infrared	solar	total
diurnal cycle	38.8	−52.4	−13.6
fixed sun	45.5	−64.3	−18.8

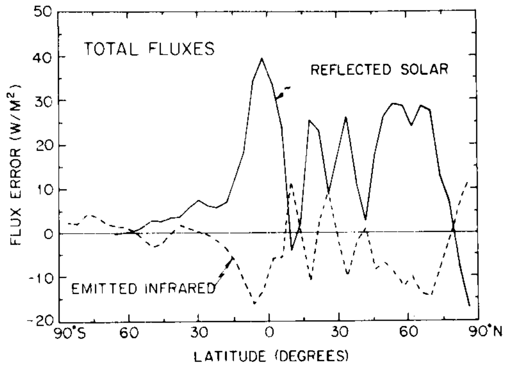

Fig. 3. Total flux errors due to use of the fixed-sun approximation. These results were obtained using the OSU/LLNL GCM.

Two additional effects contribute to the errors shown in Fig. 3; these are apparent from the errors in overcast flux shown in Fig. 4. The errors in the infrared flux are a consequence of differences in the vertical distribution of cloud cover. This also contributes to the jagged behavior of the solar error, which is superimposed upon a positive bias inherent within the fixed-sun approximation, since the OSU/LLNL GCM contains cloud reflectances which are dependent upon solar zenith angle. But the latitudinally-dependent zenith angles for the fixed-sun approximation, which produce correct diurnally-averaged insolation, do not coincide with those that would yield proper diurnally-averaged cloud reflectances. The result is an overestimate of

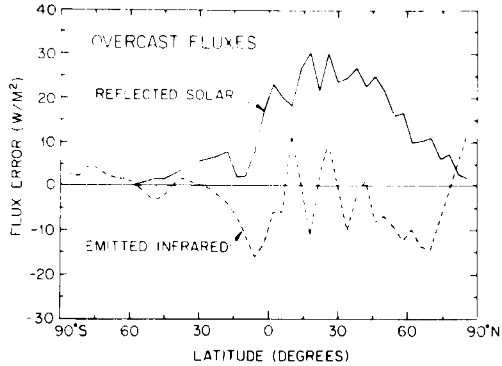

Fig. 4. Overcast flux errors due to use of the fixed-sun approximation. These results were obtained using the OSU/LLNL GCM.

reflected solar radiation. In that the ULCA GCM does not incorporate zenith-angle dependent cloud reflectances (the newer UCLA/Goddard GCM does), this source of error was not present in the study by Randall et al. (1985). The fact that we find a greater increase in planetary albedo when the diurnal cycle is suppressed (0.29 to 0.33) than did they (0.28 to 0.31) is consistent with this difference.

5. Comparison with satellite data

Conventionally, satellite-determined earth radiation budget measurements do not distinguish between clear and overcast regions, and thus they are unable to provide information on cloud radiative forcing. But recently Minnis and Harrison (1984b) employed a very clever approach in which they calibrated the GOES spin scan radiometers against radiance measurements made by the Nimbus-7 scanning radiometers. This calibration referred to simultaneous measurements for colocation of the satellites. An important point is that inherent in these calibrations are narrow-band (GOES) to broad-band (Nimbus-7) conversions.

Minnis and Harrison (1984b) were then able to employ the GOES scanners to obtain separate clear and overcast top-of-the-atmosphere solar and infrared flux measurements. A single monthly average (November 1978) was produced for a region bounded by latitude 45S to 45N and longitude 30W to 125W, corresponding to the field of view of GOES-EAST.

As we have previously emphasized, our current use of the OSU/LLNL GCM is solely for the purpose of illustrating strategies and pitfalls associated with comparisons of GCMs and earth radiation budget data. With this goal in mind, we have performed a November simulation with the OSU/LLNL GCM, averaging over a region comparable to that of the GOES data (latitude 44°S to 44°N and longitude 30°W to 125°W); comparisons with the GOES cloud forcing data are given in Table 7. An interesting point here is that the OSU/LLNL GCM can be used as a transfer vehicle for comparing the other GCMs with the GOES measurements. For example, comparison of Tables 4 and 7 crudely suggests that the modified NCAR CCM produces the best infrared cloud forcing, whereas the standard NCAR CCM and the UCLA/Goddard GCM produce the most appropriate solar forcing. Bear in mind, however, that neither version of the NCAR CCM contains a diurnal cycle.

But care must be exercised in making such comparisons, since an apparently reasonable result can actually be the product of compensating errors. As a case in point, GOES and OSU/LLNL GCM total fluxes at the top of the atmosphere are compared in Table 8, from which it is seen that the GCM is producing fairly reasonable total fluxes. But in Table 9 we additionally include the clear and overcast

Table 7. *Comparison of cloud radiative forcing as determined from GOES measurements and as predicted by the OSU/LLNL GCM*

	Cloud radiative forcing (Wm^{-2})		
Source	infrared	solar	total
GOES data Minnis & Harrison (1984b)	24.6	−57.6	−33.0
OSU/LLNL GCM	34.4	−53.6	−19.2

Table 8. *Comparison of emitted infrared and net downward solar fluxes at the top of the atmosphere as determined from GOES measurements and as predicted by the OSU/LLNL GCM*

Flux (Wm^{-2})	GOES	OSU/LLNL GCM
total Infrared	243	249
total Solar	279	289

Table 9. *Comparison of emitted infrared and net downward solar fluxes at the top of the atmosphere as determined from GOES measurements and as predicted by the OSU/LLNL GCM*

Flux (Wm^{-2})	GOES	OSU/LLNL GCM
clear infrared	267	284
overcast infrared	221	181
total infrared	243	249
clear solar	337	342
overcast solar	235	189
total solar	279	289

components of these total fluxes, and here there are obvious inconsistencies. Note that, relative to the GOES data, the GCM overestimates the total solar flux by 10 Wm^{-2}, while at the same time it underestimates the overcast solar flux by 46 Wm^{-2}. The same dilemma appears for the infrared. One would not expect the 17 Wm^{-2} overestimate of the GCM's clear flux to more than compensate for the 40 Wm^{-2} underestimate in overcast flux, but nevertheless the GCM's total infrared flux is 6 Wm^{-2} larger than the GOES total flux.

The reason for these apparent contradictions is that in order for a GCM to produce correct total fluxes, it must produce not only the correct clear and overcast components of those fluxes, but it must also calculate proper cloud amounts, and here it is errors in the latter which partially compensate for errors in the former. To be more specific, OSU/LLNL and GOES (Minnis and Harrison, 1984a) zonal cloud amounts (for longitude 30°W to 125°W) are compared in Fig. 5. The point is that the underestimates, relative to the GOES data, of the GCM overcast infrared and solar fluxes (Table 5) are partially compensated for by a corresponding underestimate in the GCM's cloud cover.

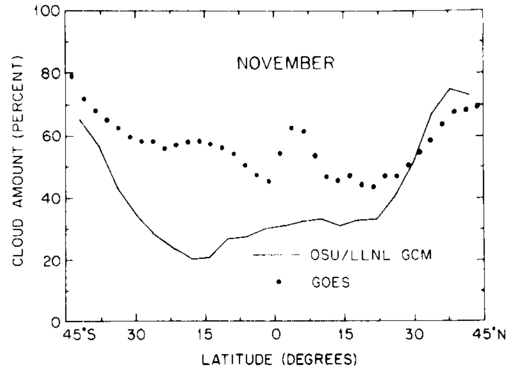

Fig. 5. Comparison of November OSU/LLNL GCM and GOES cloud amounts. These refer to zonal means averaged over longitude from 30°W to 125°W.

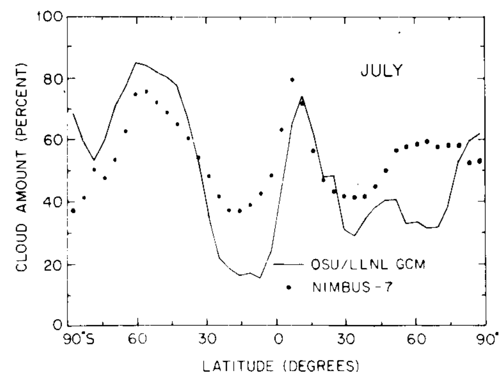

Fig. 6. Comparison of July OSU/LLNL GCM and Nimbus-7 cloud amounts. These refer to zonal means averaged over all longitudes.

From Fig. 5 one might also conclude that the GCM does not properly predict enhanced tropical cloud cover. But choosing a different month and another data set alters this conclusion. Fig 6 compares zonal mean July cloud amount, as predicted by the GCM, with that determined from the THIR (Temperature Humidity Infrared Radiometer) and TOMS (Total Ozone Mapping Spectrometer) instruments onboard the Nimbus-7 satellite for July 1979/1980 (Stowe et al., 1986). Here the model produces quite laudable tropical cloud cover, together with generally better agreement with the observations than for the November comparison. This suggests that single-month comparisons might be misleading.

The problem of compensating errors carries over to cloud forcing. To illustrate this we consider solar cloud forcing within the context of the GOES data. In terms of cloud cover fraction A_c, eq. (2) may be rephrased as

$$\mathrm{CF(solar)} \simeq A_c[S(\mathrm{overcast})\text{-}S(\mathrm{clear})] \quad (3)$$

where the approximate sign is used since this expression is strictly valid only for a single-layer cloud (Ramanathan, 1987). In addition A_c and S within eq. (3) denote monthly means for both the GCM and the GOES data, and the product of two mean values is not necessarily equal to the mean value of the product.

To circumvent these problems, we rephrase eq. (3) as

$$\mathrm{CF(solar)} = \tilde{A}_c[S(\mathrm{overcast})\text{-}S(\mathrm{clear})] \quad (4)$$

where $\tilde{A}_c$ represents an effective cloud cover fraction as defined by eq. (4) together with the GCM and GOES solar fluxes of Table 8 and the cloud forcings of Table 7. This yields $\tilde{A}_c(\mathrm{GCM}) = 0.350$ and $\tilde{A}_c(\mathrm{GOES}) = 0.565$. With these values together with the solar flux results of Table 9, we have evaluated CF(solar) for various combinations of GCM and GOES fluxes and cloud cover fractions. These are summarized in Table 10, with the top and bottom values for CF(solar) denoting the respective GCM and GOES results which, by themselves, suggest that the GCM-predicted solar cloud forcing is not substantially different from the GOES value.

But as before this apparent agreement is the result of compensating errors, since the second and third values within Table 10 represent differences due, respectively, to differences in GCM cloud cover fractions and solar fluxes. Thus, as we later emphasize, agreement of GCM-predicted cloud radiative forcing with satellite data does not, by itself, ensure that the model is correct. The point, of course, is that if a model is producing the correct cloud forcing, but for the wrong reasons, then is the model similarly correct with respect to cloud radiative feedback?

Table 10. *Comparison of solar cloud radiative forcing as calculated from GOES and OSU/LLNL GCM solar fluxes and cloud cover fractions*

Method of calculation	Solar forcing (Wm^{-2})
GCM fluxes and GCM cloud fraction	−53.6
GCM fluxes and GOES cloud fraction	−86.4
GOES fluxes and GCM cloud fraction	−35.7
GOES fluxes and GOES cloud fraction	−57.6

6. A critique of the satellite data

Although in Section 5 we have employed the GOES data (Minnis and Harrison, 1984b) as a standard against which a GCM was compared, this was done in the context of illustrating strategies and pitfalls associated with comparing GCM output to satellite data. Like GCMs, satellite data can be uncertain, and since, with certain exceptions (e.g., Slingo, 1982), modelers seldom question the data against which they compare their models, it would seem useful to briefly review the calibration traceability of the GOES data that we have utilized. As previously discussed, the GOES instruments were calibrated against the Nimbus-7 scanning radiometers using simultaneous measurements for colocation of the satellites, and we begin with the Nimbus-7 instruments.

The Nimbus-7 biaxial scanners comprise two filtered instruments that separately measure shortwave and longwave radiances, with the longwave instrument being calibrated to an onboard black body. Due to the wavelength dependence of the longwave filter, this instrument's radiance measurement depends upon the spectral characteristics of the scene it is viewing. Thus, in proceeding from calibration mode to earth-viewing mode, a spectral correction factor was employed that was determined using an atmospheric model.

The onboard black body also served as the ultimate calibration source for the shortwave scanner through the following procedure. Once the long-wave scanner was calibrated, the Nimbus-7 total (shortwave plus longwave) wide-field-of-view (WFOV) instrument was calibrated to the longwave scanner by comparing the two instruments on the nightside of the planet, integrating the scanner measurements to the field of view of the WFOV instrument. A similar procedure was then repeated on the dayside of the planet, except that here the integrated longwave scanner measurements were subtracted from the total WFOV measurements, producing "shortwave truth" to which the shortwave scanner was calibrated. As with the longwave instrument, the spectral transmittance of the shortwave scanner's detector system is strongly wavelength dependent, and this calibration procedure produced a "global" spectral correction factor. Realistically this correction factor is dependent upon the particular scene that the instrument is viewing (desert, ocean, vegetation, clouds, etc.). Recent experience with the ERBE (Earth Radiation Budget Experiment) scanners, which have a comparable detector-system spectral transmittance, indicates that scene type can introduce about a 10% variability in measured shortwave radiances if a single global correction is applied.

These Nimbus-7 scanners then served as the calibration sources for the GOES spin scan radiometers, which are narrow-band instruments with the wavelength interval of the shortwave instrument being roughly 0.55 to 0.75 μm, while that of the longwave instrument is about 10.5 to 12.5 μm. In both cases the GOES instruments were regressed against the respective Nimbus-7 instruments (Minnis and Harrison, 1984b) by performing fits of Nimbus-7 radiance measurements to GOES radiances (longwave) and the square of GOES instrument counts (shortwave).

The Nimbus-7 to GOES shortwave regression fit performed by Minnis and Harrison (1984b) is notable in that it constitutes the *first* narrow- to broad-band shortwave conversion. Previously it was conventional to simply assume that narrow-band albedo measurements were representative of broad-band quantities (e.g., Gruber and Winston, 1978; Saunders et al., 1983).

A specific virtue of the GOES measurements is that, since the satellite is geostationary, they are measurements that are made throughout the diurnal cycle, but with a corresponding restriction as to geographical domain. In contrast, most earth radiation budget measurements have been made from polar orbiters, such as Nimbus-7 which has a noon equator crossing time, and thus there is an uncertainty associated with deducing a diurnal average from limited local-time measurements. Nevertheless, one must be cognizant of the rather involved calibration traceability of the GOES instruments, particularly with respect to the shortwave measurements which additionally convolve a "global" Nimbus-7 spectral correction with a GOES spectral correction.

The point is that, as with GCM output, it is necessary to intercompare earth radiation budget data as a means of appraising the validity of the data sets. Such intercomparisons are an inherent part of the current Earth Radiation Budget experiment.

7. Summary and conclusions

The conclusions of the present paper are two-fold. First, an intercomparison of cloud radiative forcing, as predicted by six different GCMs, shows a considerable lack of agreement. Even when account is taken of differences in the models' modes of operation, there is still substantial disagreement. In view of this, it would seem hazardous to attempt, at the present time, to employ a GCM to predict cloud radiative feedback, since this is a feedback process associated with climate-induced changes in cloud radiative forcing. This does not, however, preclude the necessity of diagnosing cloud radiative feedback within a GCM as a means of understanding the model's behavior; understanding and predicting are two quite separate issues.

The second point is that comparisons of GCM output with satellite data must be made with caution, since compensating errors might easily mask inadequacies of a model. To reemphasize this important point, we selectively list in Table 11 certain of the results that were previously given in Tables 7 and 8. These comparisons, by themselves, show a reasonable degree of agreement between the satellite data and the GCM. But recall that this reasonable agreement is the consequence of compensating errors in overcast fluxes and cloud cover, as has been emphasized with respect to Tables 9 and 10.

In this regard, it should be noted that ERBE will provide, as a standard monthly product, the infrared and solar components of both the top-of-the-atmosphere total fluxes and cloud radiative forcing. Since these are the same sort of data as the selective GOES solar data given in Table 11, then the standard ERBE data products will comprise necessary but not sufficient constraints for the validation of climate models. This emphasizes the additional need for cloud climatology data sets.

And, as with earth radiation budget data, intercomparisons of cloud climatology data sets will be necessary. For example, within the context of the present study recall that the OSU/LLNL GCM produces better agreement with observed cloud cover for July (Fig. 6) than for November (Fig. 5). The question is whether this is due to a monthly preference by the GCM,

Table 11. *Comparisons of the net downward solar flux at the top of the atmosphere and the solar component of cloud radiative forcing as determined from GOES measurements and as predicted by the OSU/LLNL GCM*

Quantity (Wm^{-2})	GOES	OSU/LLNL GCM
solar flux	279	289
solar cloud forcing	−57.6	−53.6

or whether it is an artifact of using two different data sets. It would seem most useful to intercompare cloud amounts as determined from GOES and Nimbus-7 measurements. But unfortunately the Nimbus-7 data have been processed only for January and July, whereas the GOES data are available only for November.

8. Acknowledgements

We benefited from discussions with Professor V. Ramanathan concerning conceptual problems inherent in GCM and satellite data comparisons of cloud radiative forcing, and with Dr. H. Lee Kyle regarding the Nimbus-7 calibration procedure. We thank Professor W. L. Gates for his assistance and helpful discussions in conjunction with modifying the OSU GCM, Robert Mobley and A. R. Licuanan for programming assistance, and B. R. Barkstrom, Harshvardhan, M. R. Riches, M. E. Schlesinger and J. Slingo for their comments on an earlier version of this paper. We especially thank T. P. Charlock, Harshvardhan, J. F. B. Mitchell and V. Ramanathan for supplying us with their GCM results, and P. Minnis and E. F. Harrison for providing a tabulation of their GOES cloud cover fractions. M. E. Schlesinger and S. J. Ghan provided us with respective versions of the RCM. This work was partially performed under the auspices of the CO_2 Research Division, Office of Basic Energy Sciences, US Department of Energy, under Contract No. W-7405-ENG-48 to Lawrence Livermore National Laboratory and Grant No. DEFGO285ER60314 to SUNY Stony Brook, and it was supported in part by the National Science Foundation through Grant No. ATM8515310 to SUNY Stony Brook.

REFERENCES

Alexander, R. C. and Mobley, R. L. 1976. Monthly average sea-surface temperatures and ice-pack limits on a 1° global grid. *Mon. Wea. Rev. 104*, 143–148.

Briegleb, B. P., Minnis, P., Ramanathan, V. and Harrison, E. 1986. Comparison of regional clear-sky albedos inferred from satellite observations and model computations. *J. Clim. Appl. Meteorol. 25*, 214–226.

Cess, R. D. 1976. Climate change: An appraisal of atmospheric feedback mechanisms employing zonal climatology. *J. Atmos. Sci. 33*, 1831–1843.

Cess, R. D., Briegleb, B. P. and Lian, M. S. 1982. Low-latitude cloudiness and climate feedback: Comparative estimates from satellite data. *J. Atmos. Sci. 39*, 53–59.

Cess, R. D., Potter, G. L., Ghan, S. J. and Gates, W. L. 1985. The climatic effects of large injections of atmospheric smoke and dust: A study of climate feed-back mechanisms with one- and three-dimensional climate models. *J. Geophys. Res. 90*, 12937–12950.

Cess, R. D. and Ramanathan, V. 1978. Averaging of infrared cloud opacities for climate modeling. *J. Atmos. Sci. 35*, 919–922.

Charlock, T. P. 1982. Cloud optical feedback and climate stability in a radiative-convective model. *Tellus 34*, 245–254.

Charlock, T. P. and Ramanathan, V. 1985. The albedo field and cloud radiative forcing produced by a general circulation model with internally generated cloud optics. *J. Atmos. Sci. 42*, 1408–1429.

Dickinson, R. E. 1982. Modeling climatic changes due to carbon dioxide increases. In *Carbon dioxide review* (ed by W. C. Clark). New York: Clarendon, 101–113.

Ghan, S. J., Lingaas, J. W., Schlesinger, M. E., Mobley, R. L. and Gates, W. L. 1982. A documentation of the OSU two-level atmospheric general circulation model. Report 61, Climatic Research Institute, Oregon State University, Corvallis, Oreg., 391 pp.

Gruber, A. and Winston, J. S. 1978. Earth-atmosphere radiative heating based on NOAA scanning radiometer measurements. *Bull. Amer. Meteorol. Soc. 59*, 1570–1573.

Hall, M. C. G., Cacuci, D. G. and Schlesinger, M. E. 1982. Sensitivity analysis of a radiative-convective model by the adjoint method. *J. Atmos. Sci. 39*, 2038–2050.

Hartmann, D. L., Ramanathan, V., Berroir, A. and Hunt, G. E. 1986. Earth radiation budget data and climate research. *Rev. Geophys. Space Phys. 24*, 439–468.

Hartmann, D. L. and Short, D. A. 1980. On the use of earth radiation budget statistics for studies of clouds and climate. *J. Atmos. Sci. 37*, 1233–1250.

Herman, G., Wu, M. -L. and Johnson, W. 1980. The effects of clouds on the earth's solar and infrared radiation budgets. *J. Atmos. Sci. 37*, 1251–1261.

Lacis, A. A. and Hansen, J. E. 1974. A parameterization for the absorption of solar radiation in the earth's atmosphere. *J. Atmos. Sci. 31*, 118–133.

Minnis, P. and Harrison, E. F. 1984a. Diurnal variability of regional cloud and clear-sky radiative parameters derived from GOES data. Part II: November 1978 cloud distributions. *J. Clim. Appl. Meteorol. 23*, 1012–1031.

Minnis, P. and Harrison, E. F. 1984b. Diurnal variability of regional cloud and clear-sky radiative parameters derived from GOES data. Part III: November 1978 radiative parameters. *J. Clim. Appl. Meteorol. 23*, 1032–1051.

Ohring, G. and Clapp, P. 1980. The effects of changes in cloud amount on the net radiation at the top of the atmosphere. *J. Atmos. Sci. 37*, 447–454.

Paltridge, G. W. 1980. Cloud-radiation feedback to climate. *Q. J. R. Meteorol. Soc. 106*, 895–899.

Petukhov, V. K., Feygelson, Ye. M. and Manuylova, N. I. 1975. The regulating role of clouds in the heat effects of anthropogenic aerosols and carbon dioxide. *Izv. Atmos. Oceanic Phys. 11*, 802–808.

Potter, G. L. and Cess, R. D. 1984. Background tropospheric aerosols: Incorporation within a statistical-dynamical climate model. *J. Geophys. Res. 89*, 9521–9526.

Ramanathan, V. 1981. The role of ocean-atmosphere interactions in the CO_2 climate problem. *J. Atmos. Sci. 38*, 981–930.

Ramanathan, V. 1983. Modeling studies of cloud radiation feedback problems in the earth's atmosphere. The Seymour Hess Memorial Symposium, Recent Advances in Planetary Meteorology, International Union of Geodesy and Geophysics, XVIII General Asembly, Hamburg, Germany, Program and Abstracts, p. 373.

Ramanathan, V. 1985. Scientific use of surface radiation budget data for climate studies. World Climate Program Report on Surface radiation budget for climate applications, (eds.: J. T. Suttles and G. Ohring). World Meteorological Organization, Geneva, Switzerland.

Ramanathan, V. 1987. The rôle of earth radiation budget studies in climate and general circulation research. *J. Geophys. Res.*, in press.

Ramanathan, V., Lian, M. S. and Cess, R. D. 1979. Increased atmospheric CO_2: Zonal and seasonal estimates of the effect on the radiation energy balance and surface temperature. *J. Geophys. Res. 84*, 4949–4958.

Randall, D. A., Abeles, J. A. and Corsetti, T. G. 1985. Seasonal simulations of the planetary boundary layer and boundary-layer stratocumulus clouds with a general circulation model. *J. Atmos. Sci. 42*, 641–676.

Randall, D. A. and Harshvardhan 1986. Cloud radiative forcing in a general circulation. Extended Abstracts, *Sixth Conference on Atmospheric Radiation*, American Meteorological Society, Williamsburg, VA, 31–34.

Saunders, R. W., Stowe, L. L., Hunt, G. E. and England, C. F. 1983. An intercomparison between radiation budget estimates from METEOSAT 1, Nimbus-7 and TIROS-N satellites. *J. Clim. Appl. Meteorol. 22*, 546–559.

Schlesinger, M. E. 1984. Climate model simulations of CO_2-induced climatic change, *Adv. Geophys. 26*, 141–235.

Schlesinger, M. E. and Mitchell, J. F. B. 1985. Model projections of the equilibrium climatic response to increased carbon dioxide. Projecting the climatic effects of increasing carbon dioxide, (eds.: M. C. MacCracken and F. M. Luther). US Department of Energy Report DOE/ER-02037, 381 pp.

Slingo, J. 1982. A study of the earth's radiation budget using a general circulation model. *Q. J. R. Meteorol. Soc. 180*, 379–405.

Somerville, R. C. J. and Remer, L. A. 1984. Cloud optical thickness feedbacks in the CO_2 climate problem. *J. Geophys. Res. 89*, 9668–9672.

Stowe, L. L., Pellegrino, P. P., Hwang, P. H., Bhartia, P. K., Eck, T. F. and Long, C. S. 1986. Spatial and temporal characteristics of global cloud cover as observed from the Nimbus-7 satellite. Extended Abstracts, *Sixth Conference on Atmospheric Radiation*, American Meteorological Society, Williamsburg, VA, 99–102.

Wetherald, R. T. and Manabe, S. 1986. An investigation of cloud cover change in response to thermal forcing. *Clim. Change 8*, 5–23.